# Electromagnetic energy harvester with repulsively stacked multilayer magnets for low frequency vibrations

Soon-Duck Kwon[1], Jinkyoo Park[2] and Kincho Law[2]

[1] Department of Civil Engineering, Chonbuk National University, Chonju, Chonbuk, Korea. Email: sdkwon@chonbuk.ac.kr

[2] Department of Civil and Environmental Engineering, Stanford University, Stanford, CA, USA

**Abstract** : This paper investigates the applicability of an electromagnetic generator with repulsively stacked magnets for harvesting energy from traffic induced bridge vibrations. First, the governing equation for electromechanical coupling is presented. The magnetic field for repulsive pole arrangements is discussed and the model is validated from magnet falling test. The detailed design, fabrication, and test results of a prototype device are presented in the paper. Experimental vibration shaker test is conducted to assess the performance of the energy harvester. Field test and numerical simulation at the 3rd Nongro Bridge in South Korea shows that the device can generate an average power of 0.12mW from input rms acceleration of 0.25m/s$^2$ at 4.10Hz. With further frequency tuning and design improvement, an average power of 0.98mW could be potentially harvested from the ambient vibration of the bridge.

**Keywords**: energy harvesting, electromagnetic harvester, bridge vibration, linear generator, multilayer magnets.

## 1. Introduction

Wireless sensors are now broadly used for structural health monitoring application to remotely and continuously assess the conditions of civil structures [1]. Although wireless sensors are free from wires to send or receive signal, the sensors still need batteries to power. The maintenance cost for replacing batteries in wireless sensor applications can exceed the sensor's cost due to laboring fees [2]. Therefore, there has been a strong interest in developing small energy harvesting devices for powering electronic apparatus for civil infrastructure applications.

Bridges are prime candidates for application of wireless sensor based structural health monitoring system [3]. Most bridges, however, exhibit low frequency and low amplitude ambient vibration caused by either wind or traffic. Fundamental frequency of short or medium span bridges typically ranges from 2Hz to 8Hz [4], and the accelerations are generally less than $1m/s^2$. On the other hand, many vibration based energy harvesters operate with frequency over 60Hz, and they utilize harmonic oscillations induced from machinery systems [5-7].

Very few studies have been reported on energy harvesters utilizing structural ambient vibration with low frequency. Linear generator has been studied for wave energy converter which has very low frequency and high amplitude [8]. Similar concept has been applied to ambient vibration of bridges [9,10]. Two repulsively attached magnets have been used in electromagnetic oscillators to harvest energy [11,12]. Another effort has been reported using electromagnetic inertial power generator and a prototype device has been developed and applied to a medium span T-beam bridge and a long span suspension bridge [13]. However, the performance reported is quite low. The electromagnetic inertial power generator provides an average power of 0.05mW at 3.1Hz

[9] and 2.3μW at 2Hz [13].

This paper investigates the applicability of an electromagnetic generator with repulsively stacked magnets for harvesting energy from traffic induced bridge vibrations. Stacking repulsively slices of magnets can be advantageous for input vibration source with low frequency since the oscillating frequency of magnetic flux density is proportional to the number of sliced magnets. This paper is organized as follows: First, the configuration of the energy harvester with multilayers of repulsively stacked magnets and the governing equation for electrical coupling are presented. Then, the magnetic field for repulsive pole arrangements is discussed and the model is validated from magnet falling tests. The detailed design, fabrication, and experimental shaker test results of a prototype device are presented. Additionally, numerical simulation based on the prior measured bridge accelerations under ambient traffics is reported. Finally a feasibility of the proposed energy harvester concept is investigated by conducting a field test on a bridge exhibiting low frequency vibration.

## 2. Repulsively stacked multilayer electromagnetic energy harvester

### 2.1. *Description of the energy harvester*

Fig. 1(a) shows the configuration of a conventional vibration based energy harvester consisting of a single permanent magnet and a solenoid coil. Fig. 1(b) shows the configuration of repulsively stacked multilayered magnets and coils in the proposed energy harvester concept. The key idea of the multilayer device, as shown in Fig. 1(b), is that the poles of magnets are arranged to produce repellent forces of each other. The pole arrangement increases the radial component of magnetic flux density that induces inductive current in the coil, and hence the power generated.

The induced electro-motive voltage in a coil is proportional to the magnetic flux density, total coil length, and moving velocity. The use of multiple magnets, which are compactly stacked, increases the oscillating frequency of magnetic flux density as well as the flux linkage gradient. Furthermore, the oscillating frequency is proportional to the number of stacked magnets. As shown in Fig. 1(a), the sign of the magnetic flux density in a conventional single layered energy harvester changes only one time during a half cycle of oscillation. For the multilayer device, however, the sign of the magnetic flux density alternates as many times as the number of stacked magnets during the same time duration of the oscillation. As an electromagnetic energy harvester is analogous to an AC generator, the increased oscillating frequency of magnetic flux makes the multilayer system producing electrical energy more efficiently. In addition, the short axial bandwidth of the magnetic flux enables the harvester to produce electrical energy even for low amplitude vibration.

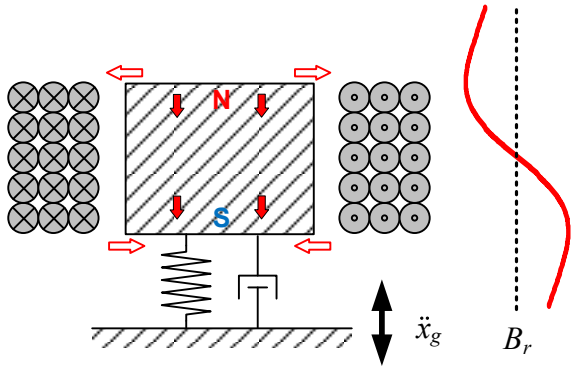


(a) Conventional single magnet and coil

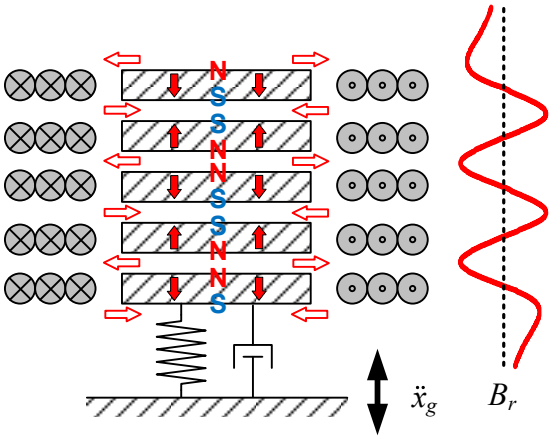


(b) Repulsively stacked multilayer magnets and independent coils

Fig. 1 Magnet structures and radial magnetic flux density of electromagnetic energy harvesters.

### 2.2. *Governing equation*

The governing equation describing the relative movement of a magnet with respective to a coil caused by base excitation can be derived from the forces acting on a system as [14,15]:

$$m_s\ddot{z}(t) + c_s\dot{z}(t) + k_s z(t) = F_{ext} + F_{em} \tag{1}$$

where $z$ denotes the relative axial displacement between the magnet and the coil, $m_s$, $c_s$ and $k_s$ are, respectively, mechanical mass, damping and stiffness. The excitation force $F_{ext}$ is given by

$$F_{ext} = -m_s\ddot{x}_g(t) \tag{2}$$

where $\ddot{x}_g$ denotes the base acceleration. The axial component of the electro-motive force $F_{em}$ opposing the motion along the coil axis can be described as a function of the induced current $I(t)$ in the coil as

$$F_{em} = \phi(z)\,I(t) \tag{3}$$

where $\phi$ is the electro-mechanical coupling coefficient related to the magnetic field which will be discussed in the next section.

For each coil $j$, the relationship between the current rate $\dot{I}_j$ , the current $I_j$ , and the relative axial speed $\dot{z}_j$ between the coil and the magnet can be written in terms of an electro-mechanical coupling coefficient $\phi_j$ , the total electric resistance $R_j$, and the inductance of the winding coil $L_{c,j}$ [16] as:

$$\dot{I}_j(t) = \frac{\phi_j(z)}{L_{c,j}} \dot{z}_j(t) - \frac{R_j}{L_{c,j}} I_j(t) \tag{4}$$

Substituting Eqs. (2) and (3) into Eq. (1), and combining it with Eq. (4), the equation of motion can be derived in a state-space form as [17]:

$$\dot{\mathbf{y}}(t) = \mathbf{A}(z)\mathbf{y}(t) + \mathbf{f}(t) \tag{5}$$

where $\mathbf{y} = \begin{bmatrix} z & \dot{z} & I_1 & \cdots & I_j & \cdots & I_n \end{bmatrix}^T$ and $\mathbf{f} = \begin{bmatrix} 0 & -\ddot{x}_g & 0 & \cdots & 0 & \cdots & 0 \end{bmatrix}^T$. In its expanded form, Eq. (5) can be expressed as:

$$\begin{bmatrix} 0 & 1 & 0 & \cdots & 0 & \cdots & 0 \\ -k_s/m_s & -c_s/m_s & -\phi_1/m_s & \cdots & -\phi_j/m_s & \cdots & -\phi_n/m_s \\ 0 & \phi_1/L_{c,1} & -R_1/L_{c,1} & \cdots & 0 & \cdots & 0 \\ \vdots & \vdots & \vdots & \ddots & \vdots & \vdots & \vdots \\ 0 & \phi_j/L_{c,j} & 0 & \cdots & -R_j/L_{c,j} & \cdots & 0 \\ \vdots & \vdots & \vdots & \vdots & \vdots & \ddots & \vdots \\ 0 & \phi_n/L_{c,n} & 0 & 0 & 0 & \cdots & -R_n/L_{c,n} \end{bmatrix} \begin{Bmatrix} z \\ \dot{z} \\ I_1 \\ \vdots \\ I_j \\ \vdots \\ I_n \end{Bmatrix} + \begin{Bmatrix} 0 \\ -\ddot{x}_g \\ 0 \\ \vdots \\ 0 \\ \vdots \\ 0 \end{Bmatrix} \tag{6}$$

Eq. (6) is a nonlinear system of equation because the electro-mechanical coupling coefficient $\phi_j$ is a function of spatially varying magnetic field surrounding the coils.

## 3. Magnetic fields

### 3.1. *Magnet moving through coil*

Considering a permanent magnet moving within a hallow circular coil as shown in Fig. 2, the mathematical representation between the motion of a magnet and the induced electro-motive voltage in a coil can be written as [18]:

$$v = \int_{l_w} B_r(z,r)dl \cdot \dot{z} \tag{7}$$

where $v$ is the induced voltage, $\dot{z}$ is the relative axial velocity between the magnet and the coil, $z$ is the relative axial distance from the center of the coil to the magnet, $r$ is the radial distance from the center of the magnet, $B_r$ is the radial component of the magnetic flux density, and $l_w$ is the total length of the coil wire inside the magnetic field. Using cylindrical coordinates, the radial component of the magnetic flux density surrounding a coil can be written as [19] :

$$B_r(z,r) = \frac{3\mu_0 m_0}{4\pi} \frac{\alpha z r}{\left[(\alpha z)^2 + r^2\right]^{5/2}} \tag{8}$$

where, $\mu_o$ is the permeability (= $4\pi\times10^{-7}$ N/A$^2$) of a vacuum, $m_0$ is the magnetic dipole moment of the magnet, and $\alpha$ is a shape adjustable factor.

The axial component of an electro-motive force opposing the motion along the coil axis follows Faraday's law of induction as [19]:

$$F_{em} = \int_{l_w} B_r(z,r)dl \cdot I \tag{9}$$

The magnitude of the electro-mechanical coupling coefficient $\phi(z,r)$ between the induced force and the electric current can be expressed as:

$$\phi(z,r) = \int_{l_w} B_r(z,r)dl \tag{10}$$

Preliminary analysis results reveal that the coupling coefficient computed using the average radius and the average axial distance is almost identical to that estimated by the integration over the coil length. Consequently, the following approximation is used to

evaluate the average coupling coefficient of a thin coil as:

$$\phi \approx B_r(z_c, r_a) l_w \tag{11}$$

where $r_a$ is the average radius of the coil, $z_c$ is the distance between the center of the magnet and the coil.

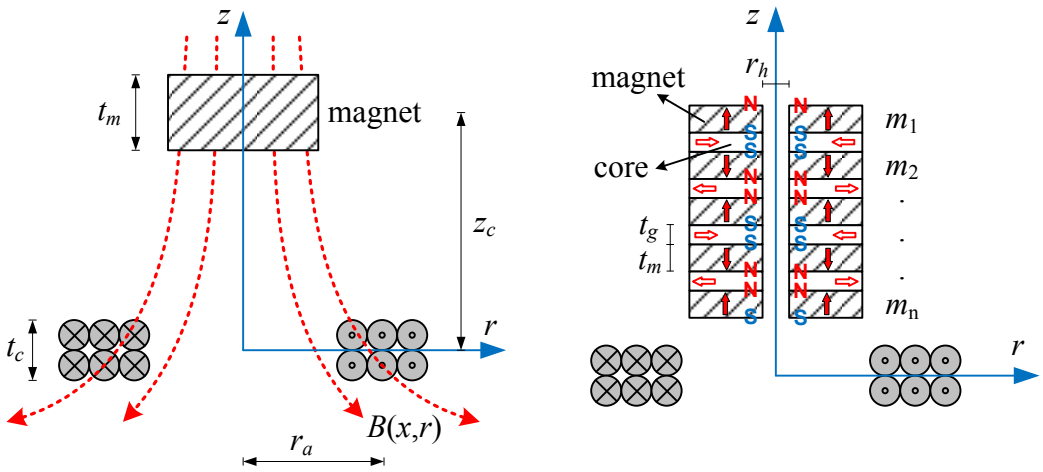


(a) Single magnet (b) Repulsively stacked magnets

Fig. 2 Pole arrangement and magnetic fields of permanent magnet moving through a coil

### 3.2. *Magnets with repulsive pole arrangements*

The magnetic field of repulsively stacked magnets shown in Fig. 2(b) has not been extensively studied. Yonnet el al. [20] computed the axial levitational stiffness of repellent magnets for a passive magnetic bearing. Coey [21] introduced a microwave power tube consisting of repulsively stacked magnets that create a periodic flux along the axis to keep the electrons moving in a narrow beam through the tube. Blache and Lemarquand [22] revealed from experiment and analysis of two repulsively stacked ring magnets that the shape of the radial component of the magnetic flux gradually changes from peak profile to triangular profile, and to sinusoidal profile as the gap width

becomes larger.

Based on the literature review, it appears reasonable to assume that for the repulsively stacked magnets, the radial component of the magnetic flux density along the magnet axis can be expressed by the superposition of each component magnet as:

$$B_r(z, r_a) = \begin{cases} \sum_{j=1}^{n} (-1)^j \frac{3\mu_0 m_0}{4\pi} \frac{\alpha z_j (r-\beta)}{\left[(\alpha z_j)^2 + (r-\beta)^2\right]^{5/2}}, & \text{for } -\frac{n}{2}(t_m + t_g) \le z \le \frac{n}{2}(t_m + t_g) \\ \frac{3\mu_0 m_0}{4\pi} \frac{\alpha z r}{\left[(\alpha z)^2 + r^2\right]^{5/2}}, & \text{otherwise} \end{cases} \tag{12}$$

where $z_j = z + (t_m + t_g)\left[j - (n+1)/2\right]$, $t_g$ is the thickness of each core (spacer), $t_m$ is the thickness of each magnet, $n$ is the number of magnets, and $\beta$ is the core factor which is zero for air core. Ferromagnetic metal core is generally used to prevent the magnetic flux from diverging in the radial direction; a metal core makes the magnetic flux concentrated in a narrow area. The effect of a metal core on the magnetic field depends on various parameters such as the core material, the geometry of core, the magnet size, etc. The usual values for the core factor is less than a quarter of magnet's diameter. The influence of the core factor and the validity of Eq. (12) will be examined from magnet falling tests to be discussed next.

### 3.3. *Magnet falling tests*

Experiments of magnet falling through a coil have been performed to verify the analytical model of magnetic fields described in Eq. (12). The experimental apparatus is shown in Fig. 3. A total number of five Neodymium magnets (NdFeB) are used in the tests. The influence of the gaps between each magnet on the inductive voltage is being

investigated by varying the gap from 1mm to 11mm. Polystyrene straw and steel washers are respectively used for an air core and a steel core to allow gaps between the ring magnets. The magnets and the cores are skewered and glued on a non-magnetic stainless steel shaft. The outer and the inner diameters of each magnet are, respectively, 9.53mm and 3.18mm, and the magnet thickness is 1.52mm. The parameters for the two different coils with different thickness used in the experiments are summarized in Table 1.

In the experiments, the magnet is simply dropped down through the coil, and the induced voltage in the coil is then measured using a data acquisition system, NI USB-6009 driver. As the magnet drops slowly, the sampling rate of 20 KHz for measuring the transient voltage is sufficient for the experimental test. The measured voltages are then normalized by the associated falling velocities by measuring the distance between magnets and the time intervals when the sign of the voltage changes. The normalized voltage based on the falling velocity is equivalent to the average electro-mechanical coupling coefficient as seen in Eqs. (7), (10) and (11).

Table 1. Coil parameters

| Parameter | Coil-A (Thin) | Coil-B (Thick) | Unit |
|---|---|---|---|
| Wire diameter | 90 | 90 | μm |
| Outer diameter | 22 | 22 | mm |
| Inner diameter | 12 | 12 | mm |
| Thickness | 2 | 4 | mm |
| Number of turns | 980 | 1960 | |
| Resistance | 145 | 290 | Ω |
| Inductance | 18.3 | 73.2 | mH |

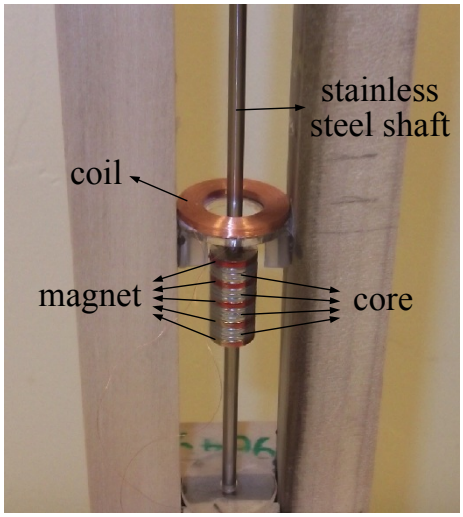


Fig. 3 Magnet falling tests

Fig. 4 shows the measured voltage from the falling tests of a single magnet and the computed voltage using Eq. (6). To understand how the induced voltage varies with the properties and the geometry of the coil, we compare the measured voltages of the two coils. Eq. (8) is applied to fit the measurements as shown in Fig. 4. It can be seen from Fig. 4 that Eq. (8) can be used to model the magnetic field of a single magnet. For coil-A (thin) and coil-B (thick), the magnetic dipole moments $m_0$ are determined respectively as 0.137 and 0.126, and the shape adjustable factors $\alpha$ are set respectively as 1.4 and 1.3 on the basis of the amplitudes and the shapes of the normalized voltage measurements. Note that the shape factors are within the range of 1.2 ~ 1.5 as reported by Donoso et al. [19].

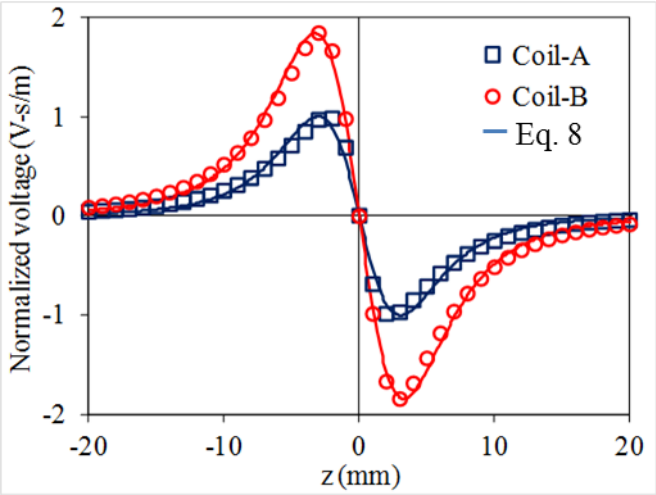


Fig. 4 Normalized induced voltages obtained from a single magnet falling through a coil

The voltage induced from the interaction between the coil and the multilayered, repulsively stacked magnets differ significantly from the case of a single magnet. In particular, the voltage wave form is affected by the core thickness (the gap distance between each magnet). Fig. 5 shows the induced voltages normalized by the speed of the falling magnet versus the air core thickness, which is adjusted using Polystyrene straw that has no influence on the magnetic flux, when five repulsively stacked magnets fall through coil-B. As noted by Blache and Lemarquand [22], the shape of magnetic flux gradually changes from a triangular profile to a sinusoidal profile and then to a saw profile as the core thickness increases.

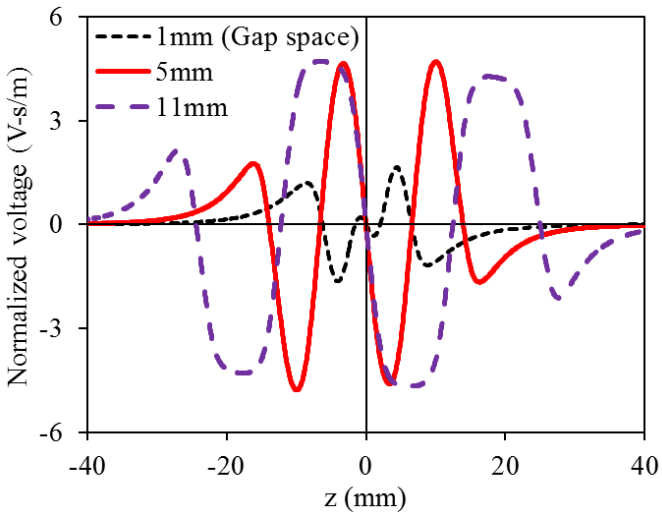


Fig. 5 Induced voltages normalized with the magnet falling speed versus thickness of air core when five repulsively stacked magnets fall through coil-B.

Steel rings are used as a spacer between the magnets, and its influence is investigated. As shown in Fig. 6(a), the coil with the steel core produces much higher voltages than the coil with air core. For the case of steel core, the voltages increase by 1.4 times when the thickness ratio between the core and the magnet is less than 2. The magnification ratio gradually increases up to 1.8 as the thickness ratio increases. The increase in voltages due to the steel core can be accounted for by adjusting the core factor $\beta$ in Eq. (12). Using a curve fitting on the measured data, as shown in Fig. 6(b), the empirical equation for the core factor when the thickness ratio between the core and the magnet is less than 7 can be expressed in terms of a flexible sigmoid function as:

$$\beta = \frac{0.72}{1+350e^{-1.4\left(t_g/t_m\right)}} + 0.84 \tag{13}$$

where $t_g$ is the thickness of each core, and $t_m$ is the thickness of each magnet.

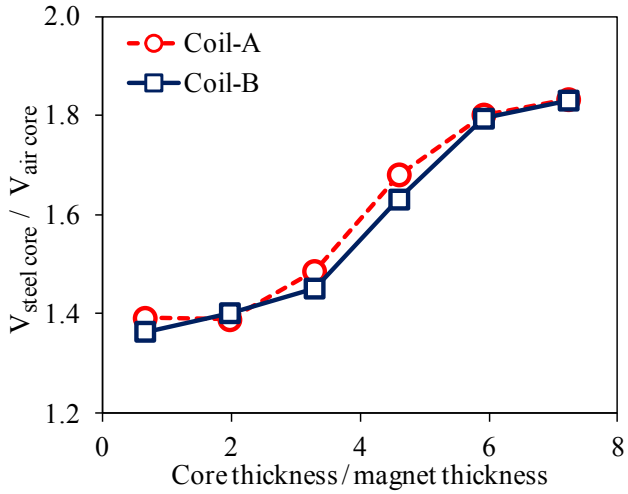


(a) Normalized induced voltages with core materials

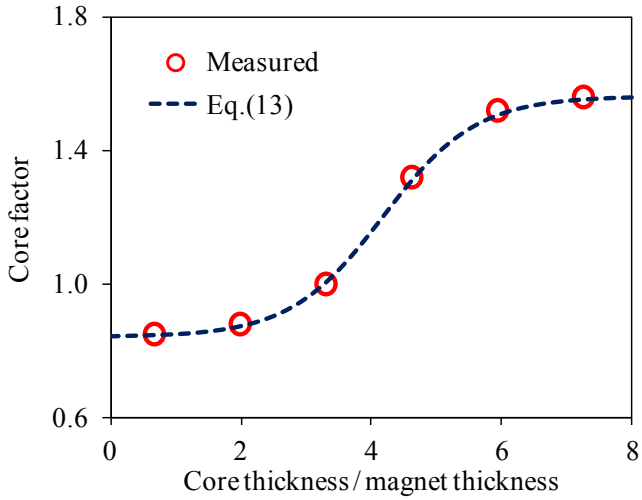


(b) Core factor versus thickness ratio of the steel core and the magnet

Fig. 6 The effect of cores on induced voltages.

The proposed magnetic flux density equation for the stacked repulsive magnets is validated through the falling magnet tests. We first plot the five independent magnetic flux density curves and then superimposed them using Eq. (12). The superimposed magnetic density is converted into normalized voltage and the results are compared to the measured voltage as shown in Fig. 7(a). Note that even though the five different magnetic flux density curves have different phases, the superimposed density curve,

labeled as Eq. (12), has the phase and the amplitude nearly identical to the measured magnetic density flux. The experiments have consequentially concluded that Eq. (12) can be effectively used for modeling the magnetic flux density for the multilayered, repulsively stacked magnets configuration. As noted earlier, the proposed equation for the empirical core factor is incorporated into Eq. (12) for the case of a steel core. As shown Fig. 7(b), the normalized voltage on superimposing the measured magnetic density curves with steel core also compare favorably with Eq. (12) with the core factor $\beta = 1$. It can be seen that the voltage increase of the proposed multilayered system compared to the single magnet is quite noticeable. Furthermore, the interface with electrical circuits using the multi-layered devise as proposed is easier than the single magnet system due to its higher voltage output.

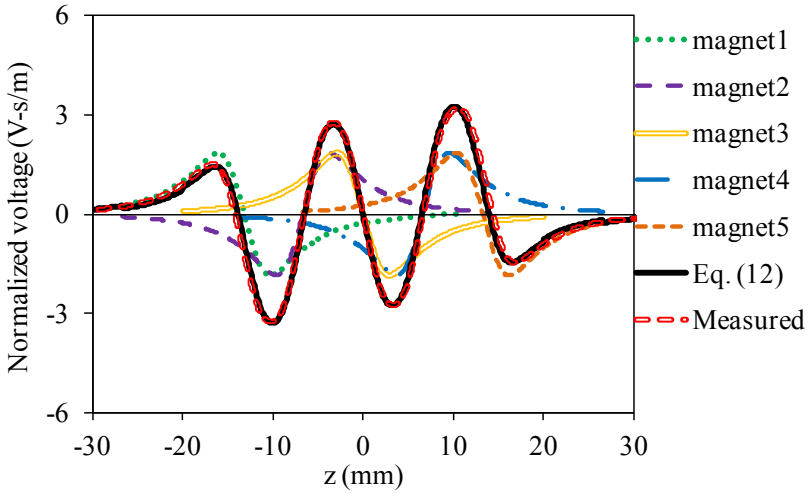


(a) Air core with thickness of 5mm ($\beta$=0)

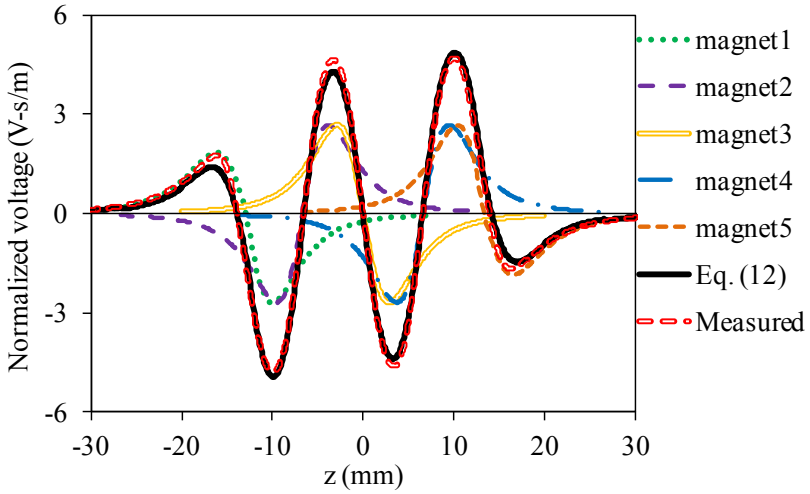


(b) Steel core with thickness of 5mm ($\beta$=1)

Fig. 7 Combination of five individual magnetic densities to produce repulsive magnetic structure around coil-B

## 4. Energy harvesting from low frequency vibrations-Laboratory experiments

Fig. 8 shows the prototype of an energy harvesting device consisting of coils and repulsively stacked magnets. The two coils in the device are the same as coil-B whose parameters are tabulated in Table 1. There are eight Neodymium (NdFeB) ring magnets and seven steel cores which are skewered and glued on the stainless steel shaft. The thickness of each steel core is 5mm. Therefore, the distance between the centers of a pair of magnets is 6.52mm. The dimensions and the parameters of the coils and the magnets are the same as those used at the falling magnet tests described earlier.

The housing containing the two coils and a proof mass is made of acrylonitrile-butadiene-styrene (ABS) copolymer. Three strips of polytetrafluoroethylene (PTFE) sheet are glued to the magnet stack to reduce friction loss. Lead nuggets are added at the top of the coil to adjust the mass. The total mass of the moving part is 56g.

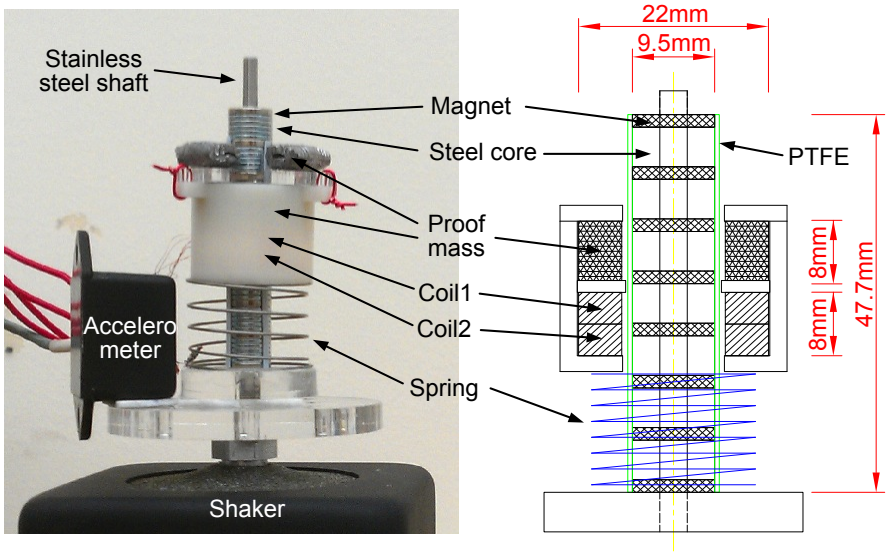


Fig. 8 Experimental setup with prototype

Shaker tests have been carried out to verify the dynamics and performance of the prototype device, and to validate the numerical model. Fig. 8 depicts the experimental setup. In the experiment, the base excitation is provided by a vibration shaker (Modal Shop, K2007E01) and the response is measured by an accelerometer (Crossbow, CXL02LF1). The induced voltages are measured by the data acquisition device (National Instrument USB-6009). In the test, the electric load resistance $R_L$ was changed from 0Ω to 5000Ω in order to vary the total resistance of the system and to dissipate the harvested electric power with a closed circuit.

To evaluate the dynamic properties of the prototype harvester, the rms voltage is measured by varying the periodic excitation frequency using the shaker. The constructed transfer function showing the relationships between the rms voltage and the excitation frequency reveals that the natural frequency and the damping ratio of the prototype harvester are 3.65 Hz and 2.3 %, respectively. Note that the voltage is measured using USB-6009 whose internal resistance is 144 KΩ.The rms voltage is measured by

changing the load resistance $R_L$. The results show that the generated power reaches its maximum when the $R_L$ is 680 Ω.

Given the natural frequency of the harvester and the optimal load resistance, the power performance curve can be constructed as a function of the excitation frequency (fixing $R_L$= 680 Ω) and as a function of the load resistance (fixing the excitation frequency at 3.65 Hz with a rms acceleration of 0.53m/s$^2$) as shown in Figs. 9a and 9b, respectively. Fig. 9a shows that the voltage increases with the load resistance and reaches its maximum near the load resistance of 680Ω. This value is comparable to the optimal resistance of 660Ω obtained from electric resistance matching (maximum power is produced when the coil resistance $R_C$ is equal to the load resistance $R_L$) [24].

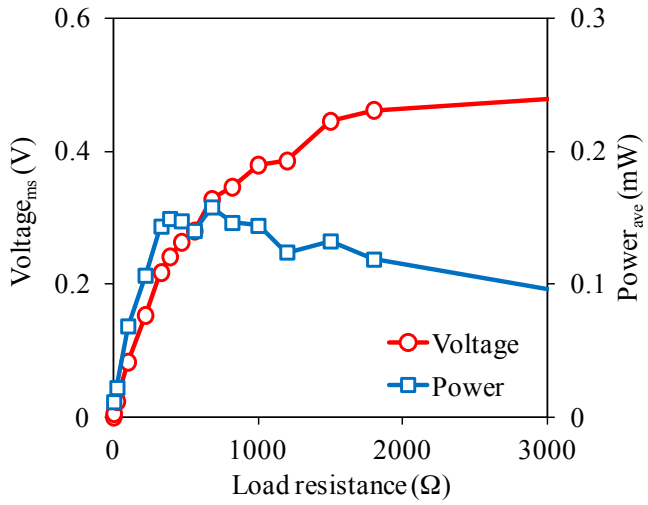


(a) RMS voltage and average power per coil at 3.65Hz frequency

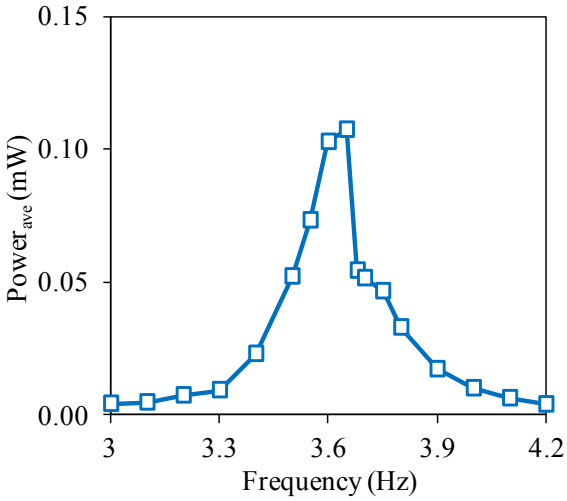


(b) Average power per coil with 680Ω load resistance

Fig. 9 Measured voltage and power across load resistance at single coil for the rms acceleration of 0.53m/s$^2$.

In order to compare the measured and simulated voltages, Eq. (5) is solved numerically by using the measured base acceleration of the shaker as shown in Fig. 10(a). As shown in the figure, due to the limitation of the shaker in exciting pure wave form at low frequency range, signal noises are inherent in the measurements. Nevertheless, as shown in Figs. 10(b) and 10(c), the simulated voltage shows good agreement with the measured results. Note that the wave form of the measured voltages for the coil 2 is slightly different from that for the coil 1. The difference is due to the their positions: the coil 2 is located on the top of the coil 1, leading the coil 2 to experience less magnetic flux than the coil 1 when they oscillate vertically.

The average powers obtained from the measured and the simulated results are, respectively, 0.156mW and 0.144mW. The results demonstrate the effectiveness of the proposed models for magnetic field and electro-mechanical coupling as discussed earlier.

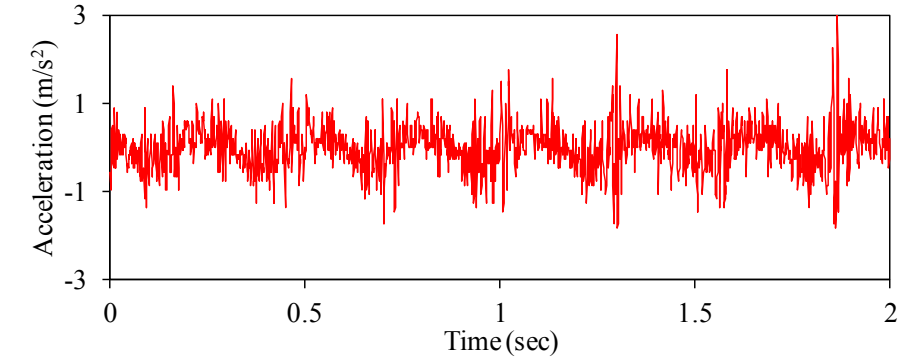


(a) Base acceleration measured at shaker

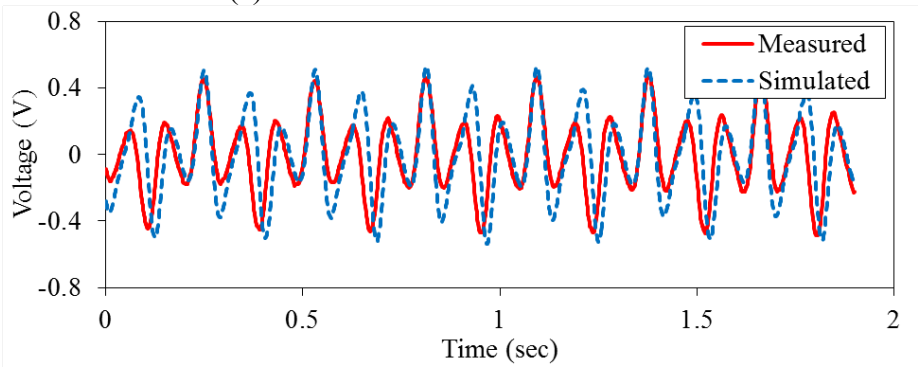


(b) Voltages at the Coil 1

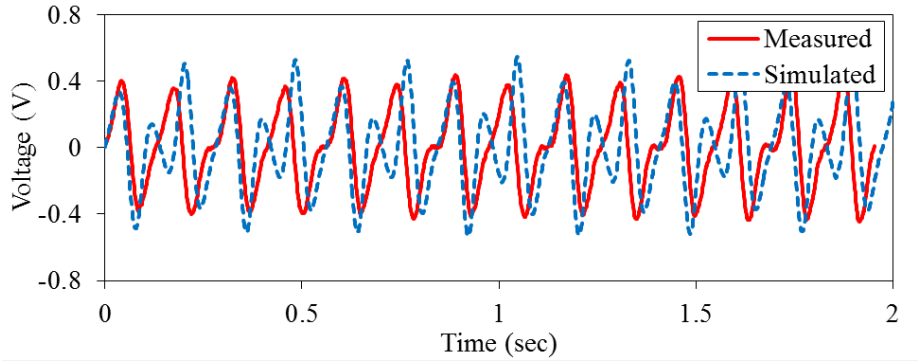


(c) Voltages at the coil 2

Fig. 10 Wave forms obtained with shaker tests.

## 5. Energy harvesting from low frequency vibrations-Numerical simulations

To investigate the feasibility of power generation from low frequency vibrations, numerical simulation is conducted to estimate the power generated using the prototype device. Specifically, the recorded vertical girder acceleration at the 5$^{th}$ Nongro Bridge in Korea shown in Fig. 11 is used in the simulation [25]. The bridge was located in a rural area with relatively low traffic. Figs. 12(a) and 12(b) show the measured acceleration

over a period of 10 minutes. The acceleration signals indicate there were 25 vehicles crossing the bridge during the 10 minutes period. The peak acceleration measured is about 1.33 $m/s^2$, and the standard deviation on the 10 minute acceleration is 0.144 $m/s^2$. As shown in the power spectrum plot in Fig. 12(b), the estimated fundamental frequencies of the vertical and the torsional modes are 2.39Hz and 3.17Hz, respectively.

Numerical simulation is conducted by solving Eq. (5) using the parameters of the prototype device as described in Table 1 and the acceleration record. It was assumed that the natural frequency of the device is tuned to the first-mode fundamental frequency of the bridge (2.17Hz) and, furthermore, the damping ratio is reduced to 1% for the numerical simulations to represent the ideal case. Figs. 13(a) and 13(b) show the numerically simulated results on the voltages and the powers. As shown in Table 2, the peak and the average power obtained from bridge vibration are respectively 5.07mW and 0.12mW over the 10-minute period. The numerical simulation shows the feasibility in extracting power from low frequency bridge vibrations. In general, the power produced by the device depends on traffic flows, and the device should be able to generate more power with the increase in traffics and vehicle speed.

Fig. 11 The 5th Nongro Bridge, located in Kimhae-si, South Korea (demolished 2006)

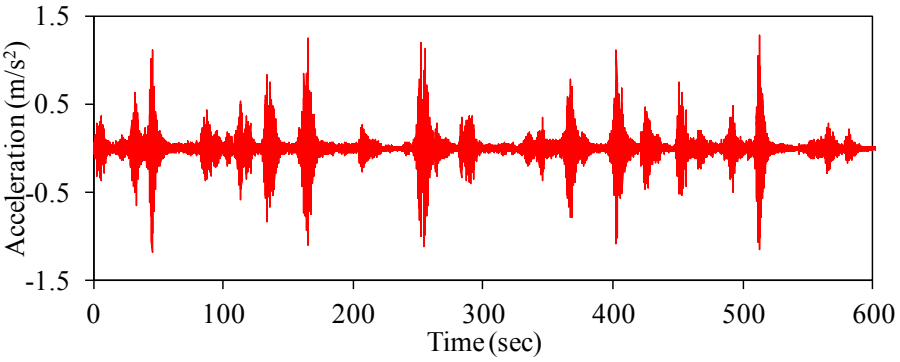


(a) Girder acceleration

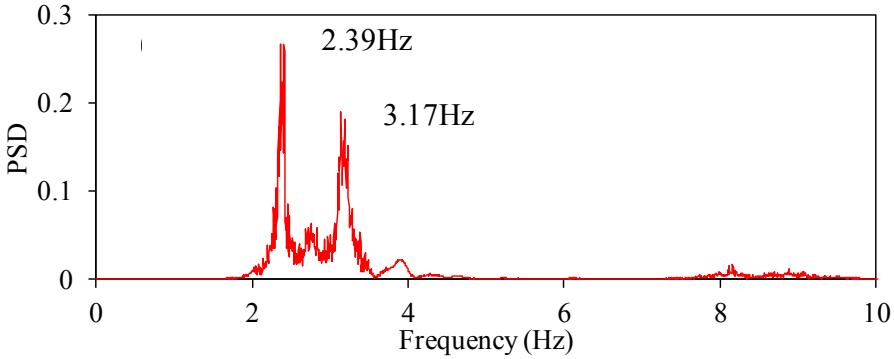


(b) Power spectrum density

Fig. 12 Recorded bridge acceleration

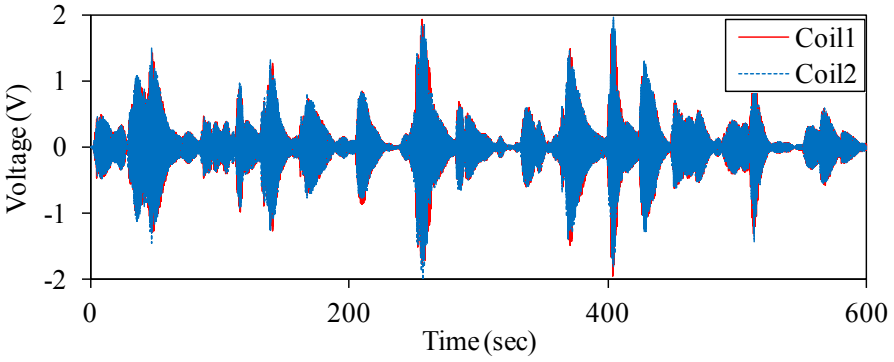


(a) Voltage

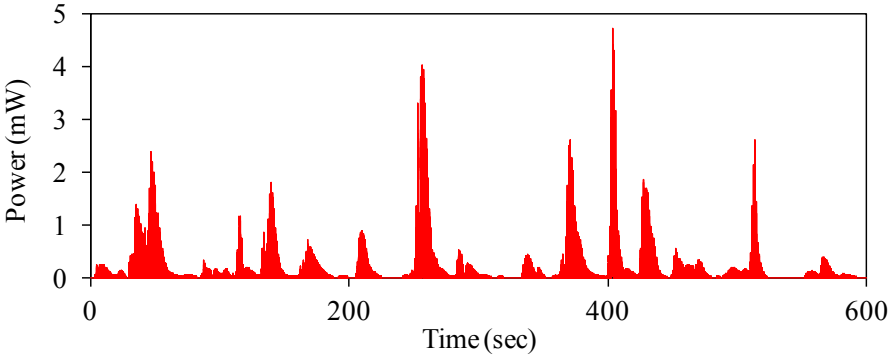


(b) Power

Fig. 13 Simulation results

Table 2. Simulation results

| | | Coil1 | Coil2 |
|---|---|---|---|
| Voltage (V) | Peak | 2.096 | 2.093 |
| | Standard deviation | 0.263 | 0.263 |
| Power (mW) | Peak | 3.850 | 3.860 |
| | Average | 0.060 | 0.060 |
| | Total average | 0.120 | |

## 6. Field Tests

The numerically simulated energy harvester power production using the recorded bridge acceleration assumes two ideal conditions in the prototype device: i) perfect frequency tuning and ii) lower structural damping. To verify that the prototype energy harvester actually generates power utilizing ambient bridge vibration and that the proposed analytical models are valid, a field experiment is being conducted at the 3rd Nongro Bridge in Pusan, Korea, shown in Fig. 14(a). Since the bridge used for numerical simulation has been demolished, the 3rd Nongro Bridge having a similar structural system is used instead. The field test allows us to identify the limitations in applying vibration-based energy harvesters to civil structures and the possible improvements necessary for increasing the performance of the prototype device.

Figs. 14(a), 14(b), and 14(c) show, respectively, the concrete bridge deck, the installed prototype and the data acquisition systems, and the heavy-loaded truck passing over the bridge. The time series of the bridge acceleration and its power spectrum density are shown, respectively, in Figs. 15(a) and 15(b). Fig. 15(a) shows the acceleration time series measured when the heavy-loaded truck was crossing the bridge. The measured peak acceleration is about 1 $m/s^2$, and the standard deviation of the 10-sec long acceleration is 0.250 $m/s^2$. As shown in Fig 15(b), the natural frequencies of the

bridge are identified as 2.74Hz and 4.10Hz, respectively. The natural frequency of the prototype device is 3.65Hz and, therefore, is not tuned to the natural frequencies of the bridge.

(a) The 3rd Nongro bridge

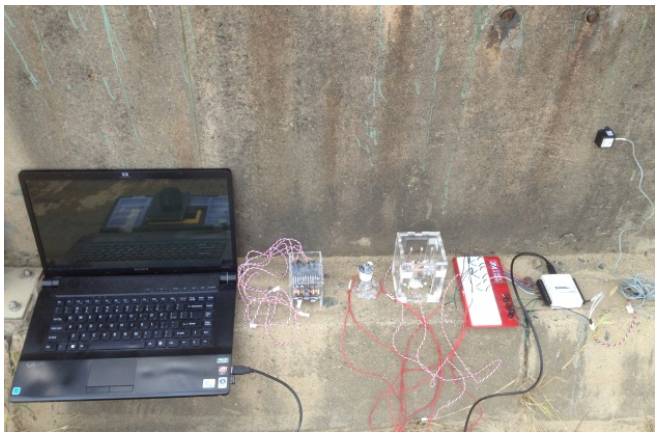

(b) Installed prototype device and Data acquisition

(c) Heavy load vehicle

Fig. 14 Field test

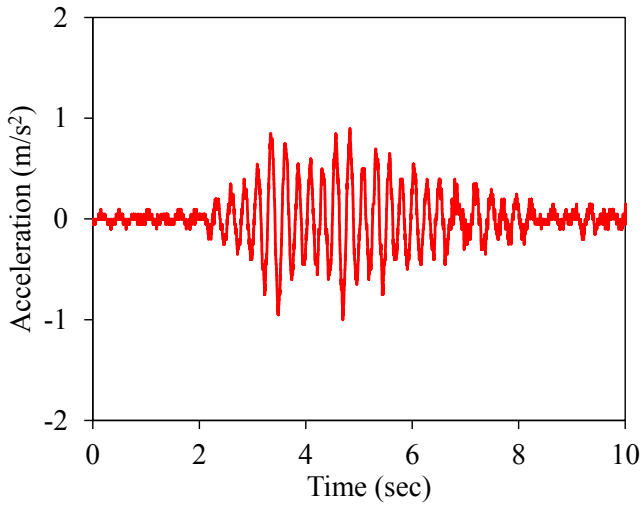


(a) Slab acceleration

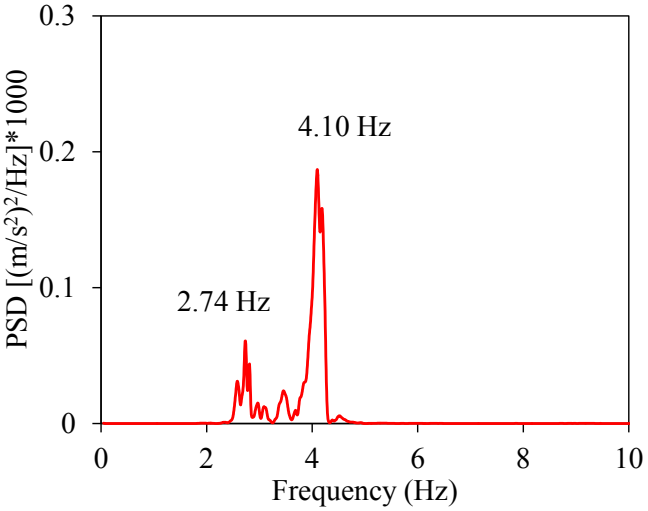


(b) Power spectrum density

Fig. 15 Recorded bridge vibration

Figs. 16(a) and 16(b) show the measured and the simulated voltages and the power time series from the coil 1 in the prototype device. The peak and the average power for the coil 1 are 0.75mW and 59μW respectively, for the duration of 10 seconds when the heavy loaded truck passes. For comparison, the numerical simulations are also conducted using the measured bridge acceleration as an input to Eq. (5). The simulated results compare favorably with the measured voltages and the powers in terms of amplitude and phase.

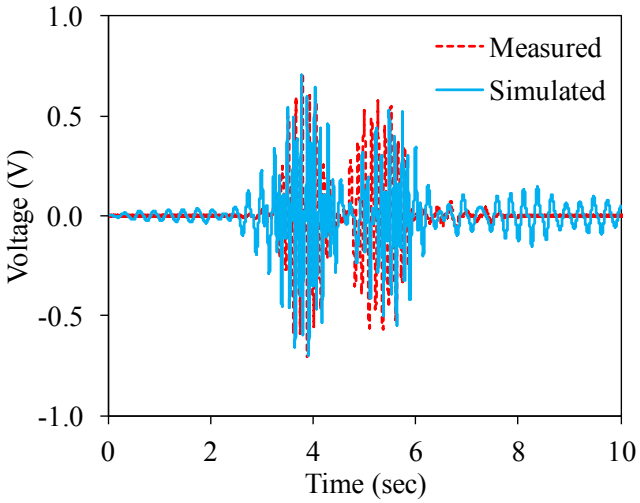


(a) Voltage

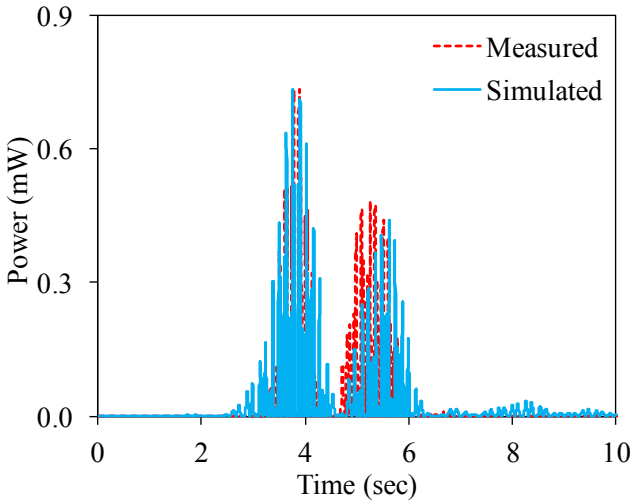


(b) Power

Fig. 16 Test and simulation results for coil 1

The efficiency of the prototype device can be improved by tuning the natural frequency and by reducing the structural damping ratio. The influence of the frequency tuning and the damping reduction on the performance of the prototype device is investigated using numerical simulations. First, the corresponding power is estimated, assuming that the natural frequency of the device is perfectly tuned to the fundamental frequency of vertical vibration of the bridge. The results show that the peak and the average power per coil increase up to 1.68mW and 0.24mW, respectively. The average power increases by almost four times due to resonance. Furthermore, the numerical

simulation is conducted with an additional condition that the structural damping ratio is reduced down to 1 %. The results reveal that the peak and the average power per coil can increase up to 3.43mW and 0.49mW, respectively. Table 3 summarizes results for the field tests and numerical simulations. Table 4 shows a comparison of the power density of different energy harvesters reported in the literature for low frequency vibrations where the natural frequency is less than 10Hz. The power density is defined as the harvested power divided by total volume of the device as a measure to compare the efficiency of the harvesters. The device shows fairly good performance even when the system is not tuned to the vibrational frequency of the target bridge. With fine tuning and design improvements, the device performance is superior than those reported.

Table 3. Test and simulation results for a single coil (coil 1)

| Case | Inherent property | | Voltage/coil | | Power/coil | |
|---|---|---|---|---|---|---|
| | frequency (Hz) | damping (%) | peak (V) | rms (V) | peak (mW) | average (mW) |
| Field test | 3.65 | 2.3 | 0.71 | 0.14 | 0.73 | 0.06 |
| Simul-A[a] | 3.65 | 2.3 | 0.71 | 0.14 | 0.73 | 0.05 |
| Simul-B[b] | 4.10 | 2.3 | 1.07 | 0.30 | 1.68 | 0.24 |
| Simul-C[c] | 4.10 | 1.0 | 1.54 | 0.45 | 3.43 | 0.49 |

[a] Simul-A refers the numerical simulation using the measured bridge acceleration time series without ideal assumptions.
[b] Simul-B indicates the numerical simulation with the assumption that the natural frequency of the device is tuned to the bridge fundamental frequency.
[c] Simul-C represents the numerical simulation with the damping ratio reduced to 1%.

Table 4. Summary of energy harvesters (natural frequency less than 10Hz)

| Reference | Frequency (Hz) | Acceleration ($m/s^2$) | | Power (μW) | | Total volume ($cm^3$) | Power density ($\mu W/cm^3$) | Method | Test |
|---|---|---|---|---|---|---|---|---|---|
| | | peak | rms | peak | average | | | | |
| Tashiro [25] | 6.0 | | | 36 | | 15.0 | 2.42 | electrostatic | |
| Arakawa [26] | 10.0 | 3.95 | | 6 | | 0.4 | 15.00 | electrostatic | |
| Elvin [27] | 8.7 | 3.10 | 0.61 | | 0.25 | 0.101 | 2.47 | piezoelectric | earthquake |
| Khaligh [28] | 2.0 | 4.73 | 3.34 | 43000 | | | | Piezoelectric+ electromagnetic | |
| Jung [29] | 2.8 | | 0.75 | | 24400 | 1244.1 | 19.61 | electromagnetic | shaker |
| Sazonov [10] | 3.1 | 3.79 | 2.68 | 12000 | | | | electromagnetic | |
| Galchev [13,30], | 10.0 | 9.80 | | 163 | 13.6 | 4.8 | 2.85 | electromagnetic | shaker |
| | 2.0 | 0.54 | | 57 | 2.3 | 68.0 | 0.03 | electromagnetic | shaker |
| | < 1 | | | | 0.7 | 68.0 | 0.01 | electromagnetic | field |
| Proposed device | 3.7 | 1.00 | 0.25 | 1500 | 118 | 18.1 | 6.51 | electromagnetic | field (not tuned) |
| | 4.1 | 1.00 | 0.25 | 6860 | 980 | 18.1 | 54.05 | electromagnetic | field (ideally tuned) |

## 5. Conclusions

This paper presents the design, fabrication and validation of an electromagnetic generator with repulsively stacked magnets for harvesting energy from traffic induced low frequency bridge vibrations. The electromechanical coupling model is validated from magnet falling tests and shown to be an effective model for evaluating the power performance of electromagnetic energy harvesters. Numerical simulations have been conducted to show the feasibility of the prototype energy harvesting device. The prototype device has been tested in laboratory experiments and in the field to demonstrate its potential in producing power utilizing low frequency structural vibrations. Further fine frequency tuning to the dominant frequency of the target bridge and lowering structural damping, for example, by reducing the friction between the steel shaft and the coil container house in the prototype device can further improve the power production of the multilayered repulsively stacked magnetic energy harvesting device.

**Acknowledgement**

This work is performed during the first author's sabbatical stay at Stanford University. The first author gratefully acknowledges the support of oversea research fund by Chonbuk national University, and of the grant (11CCTI-A052604-04) from the Ministry of Land, Transport and Maritime of Korean government. This research is partially supported by the US National Science Foundation under Grant No. CMMI-0824977. Any opinions, findings, and conclusions or recommendations expressed in this material are those of the authors and do not necessarily reflect the views of the National Science Foundation.

**Appendix : Nomenclature**

$B$ : magnetic flux density

$F_{\text{em}}$ : axial component of electro-motive force.

$F_{\text{ext}}$ : the excitation force.

$i$ : the induced current in coil

$l_w$ : total length of wire inside magnetic field

$m_0$ : the magnetic dipole moment of the magnet.

$m_s$, $c_s$ and $k_s$ : mechanical mass, damping and stiffness respectively

$r$ : radial distance from magnet axis to coil

$r_a$ : average radius of coil,

$t_g$ : thickness of each core

$t_m$ : thickness of each magnet

$\ddot{x}_g$ : base acceleration

$z$ : relative distance between magnet center to coil center

$z_c$ : distance from magnet to coil center

$\beta$ : core factor

$\alpha$ : shape adjustable factor

$\phi$ : magnetic field

$\mu_0$ : the permeability of vacuum (= $4\pi\times10^{-7}$ N/A$^2$)

**References**


[1] Lynch J P, Wang Y, Law K H, Yi J H, Lee C G and Yun C B (2005), "Validation of a large-scale wireless structural monitoring system on the Geumdang Bridge," *International Conference on Safety and Structural Reliability*, Rome, Italy, PP. 19-23.

[2] Low-Cost Vibration Power Harvesting for Wireless Sensors, U.S. Department of Energy, Energy Efficiency and Renewable Energy, available: http://www1.eere.energy.gov/industry/sensors_automation/pdfs/kcf_vibrationpower.pdf.

[3] Williams C B, Pavic A, Crouch R S and Woods R C (1997), "Feasibility study of vibration-electric generation for bridge vibration sensors," *IMAC-XVI*, PP. 1111-1117.

[4] Bachmann H and Ammann W (1987), *Vibrations in Structures induced by man and machines*. IABSE Structural Engineering Document 3e, International Association for Bridge and Structural Engineering, Zurich.

[5] Roundy S, Wright P K and Rabaey J (2003), "A study of low level vibrations as a power source for wireless sensor nodes," *Computer Communications* 26(11): 1131-1144.

[6] Beeby S P, Torah R N, Tudor M J, Glynne-Jones P, O'Donnell T, Saha C R and Roy S (2007), "A micro electromagnetic generator for vibration energy harvesting ," *J. of Micromechanics and Microengineering,* 17(7): 1257-1265.

[7] Oliver J M and Priya S (2009), "Design, fabrication, and modeling of a four-bar electromagnetic vibration power generator," *J. of Intelligent Material Systems and Structures,* 21: 1303-1316.

[8] Leijon M, Bernhoff H, Agren O, Isberg, J, Sundberg J, Berg M, Karlsson K E and Wolfbrandt A (2005), "Multiphysics simulation of wave energy to electric energy conversion by permanent magnet linear generator," *IEEE Transaction on Energy Conversion,* 20(1): 219-224.

[9] Li H and Pillay P (2008), "A methodology to design llinear generators for energy conversion of ambient vibrations," *IEEE 43nd Industry Applications Conference*, Edmonton, 1-8.

[10] Sazonov E, Li H and Pillay P (2009), "Self-powered sensors for monitoring of highway bridges," *Sensors Journal, IEEE,* 9: 1422-1429.

[11] Saha C R, Donnell T O, Wang N and McCloskey P (2008), "Electromagnetic generator for harvesting energy from human motion," *Sensors and Actuators, A,* 147: 248-253.

[12] Dayal R, Dwari S and Parsa L (2011), "A new design for vibration-based electromagnetic energy harvesting systems using coil inductance of microgenerator," *IEEE Transactions on Industry Applications,* 47(2): 820-830.

[13] Galchev T, McCullagh J, Peterson R L and Najafi K (2011) "Harvesting traffic-induced vibrations for structural health monitoring of bridges," *J. of Micromechanics and Microengineering,* 21: 1-13.

[14] Priya S and Inman D J (2009), *Energy Harvesting Technologies*, Springer, 129-161.

[15] Kamierski T J and Beeby S P (2010), *Energy Harvesting Systems: Principles, Modeling and Applications,* Springer, 1-77.

[16] Sinha P K (1987), *Electromagnetic Suspension - Dynamics and Control*, IEE, London.

[17] Lee J S, Kwon S D, Kim M Y, Yeo I (2009), "A parametric study on the dynamics

of urban transit maglev vehicle running on flexible guideway bridges," *J. of Sound and Vibration,* 328(3): 301-317.

[18] Bedekar V, Oliver J and Priya S (2009), "Pen harvester for powering a pulse rate sensor," *J. of Physics D: Applied Physics,* 42: 1-9

[19] Donoso G, Ladera C L and Martin P (2009), "Magnet fall inside a conductive pipe: motion and the role of the pipe wall thickness," *European Journal of Physics,* 30: 855-869

[20] Yonnet J P, Lemarquand G, Hemmerlin S and Olivier-Rulliere E (1991), "Stacked structures of passive magnetic bearings," *J. of Applied Physics,* 70: 6633-6636.

[21] Coey J M D (2002), "Permanent magnet applications," *J. of Magnetism and Magnetic Materials,* 248: 441–456

[22] Blache C and Lemarquand G (1992), "New structures for linear displacement sensor with high magnetic field gradient," *IEEE Transaction on Magnetics,* 28: 2196-2198

[23] MacLatchy C S, Backman P and Bogan L (1993), "A quantitative magnetic braking experiment," *American Journal of Physics,* 61(12): 1096-1101.

[24] Stephen N G (2006), "On energy harvesting from ambient vibration," *J. of Sound and Vibration,* 293: 409–425.

[25] Tashiro R, Kabei N, Katayama K, Ishizuka Y, Tsuboi F, and Tsuchiya K (2002), "Development of an electrostatic generator that harnesses the ventricular wall motion," *Japan Society of Mechanical Engineers International Journal. Series C*, 5: 239–245.

[26] Arakawa Y, Suzuki Y, and Kasagi N (2004), "Micro seismic electret generator using electret polymer film," *4th International Workshop Micro and*

*Nanotechnology for Power Generation and Energy Conversion Application*, 187–190.

[27] Elvin N G, Lajnef N and Elvin A A (2006), "Feasibility of structural monitoring with vibration powered sensors," *Smart Material and Structures,* 15(4): 977–986.

[28] Khaligh A, Zeng P, Wu X and Xu Y (2008), "A hybrid energy harvesting topology for human-powered mobile electronics," *34th Annual Conference of IEEE Industrial Electronics*, Orlando, 448–453.

[29] Jung, H J, Kim I H and Jang S J (2011), "An energy harvesting system using the wind-induced vibration of a stay cable for powering a wireless sensor node," *Smart Material and Structures*, 20: 1-9.

[30] Galchev T, Kim H and Najafi K, (2011), "Micro power generator for harvesting low-Frequency and nonperiodic vibrations, Journal of Microelectromechanical Systems, 20(4): 852-866.